ELSEVIER

International Journal of Heat and Fluid Flow 20 (1999) 341–348

International Journal of HEAT AND FLUID FLOW

www.elsevier.com/locate/ijhff

Modeling turbulent diffusion in a rotating cylindrical pipe flow

A.F. Kurbatskii, S.V. Poroseva *

Institute of Theoretical and Applied Mechanics, Siberian Division of Russian Academy of Sciences, 630090 Novosibirsk, Russia

Abstract

The influence of accuracy of the turbulent diffusion model (TDM) included in the Reynolds stress transport model (RSTM), on describing the behavior of the mean velocity components as well as the Reynolds stresses has been studied for an isothermal incompressible flow in a rotating cylindrical pipe. RSTMs used usually in practice, cannot reproduce correctly the behavior of statistical characteristics along the rotating pipe axis, in particular. Because of strong inhomogeneity of the flow, one of the reasons of the RSTM shortcomings could be insufficient accuracy of TDMs. A new tensor-invariant model for the triple velocity correlations, describing satisfactorily their behavior over the whole flow field, from the pipe axis to the wall, has been developed by the authors. Testing the standard RSTM with the different TDMs in a rotating pipe flow shows that for calculating the first- and second-order moments, the important characteristic of the TDM is its tensor-invariance. The mean velocity components are mostly influenced by the model for the pressure–strain correlations. Application of more accurate TDM creates the basis to improve models for the pressure–strain correlations and the dissipation tensor, and, finally, get the RSTM applicable to a wide range of turbulent flows.

Keywords: Turbulence; High-order modeling; Swirling flow

Notation

U_i, u_i	covariant components of mean and fluctuating velocities
$f_{,i}$	differential operator defined by $\partial f/\partial x_i$
x_i	coordinates
x_n	normal distance to a pipe wall
g^{ij}	metric tensor
D/Dt	mean substantial derivative
$\langle\cdots\rangle$	means ensemble averaging
r, x	radial and axial coordinates
R, D	pipe radius and diameter
U, W	longitudinal and circumferential components of mean flow velocity
u, v, w	longitudinal, radial, and circumferential components of fluctuating velocity
u_{*o}	friction velocity
W_o	rotating pipe wall velocity
U_m	mean axial flow velocity
U_o	mean velocity at pipe center
$N = W_o/U_m$	swirl parameter
$k = (1/2)\langle u_i^2\rangle$	turbulent kinetic energy
$\tilde{P}$, p	mean pressure and pressure fluctuation
δx	forward-step in the grid
Ri	Richardson number
$Re_m = U_m D/\nu$, $Re_o = U_o D/\nu$, $Re_* = u_{*o} R/\nu$	Reynolds numbers
$S(u_i) = \langle u_i^3\rangle/\langle u_i^2\rangle^{3/2}$	skewness factor
$Ku = \langle u^2\rangle(N\rangle 0)/\langle u^2\rangle(N=0)$	damping coefficient
$y_+ = (1 - r/R)Re_*$	

Greek

ε	dissipation rate of turbulent kinetic energy
ρ	flow density
ν	kinematic viscosity
$\tau = \kappa/\varepsilon$	time scale of the velocity field
δ_{ij}	Kronecker symbol

1. Introduction

Turbulent swirling flows are widely used in modern technological processes and occur in the natural environment as large-scale concentrated vortex formations. Rotation in such flows has a strong influence on turbulent momentum, heat, and mass transport.

The influence of rotation on the flow structure is determined, among other factors, by the way vorticity is produced. In the present work, a turbulent incompressible isothermal flow in a rotating straight cylindrical pipe is considered. Such flow is of interest because it occurs in various engineering systems, like, e.g., heat exchangers and rotor cooling systems.

* Corresponding author. E-mail: poroseva@gas.nsu.ru.

0142-727X/99/$ – see front matter
PII: S0142-727X(99)00009-0

Moreover, such type of a turbulent flow has all the features of boundary-layer flows of practical interest, whose rotation is caused by a rotating surface. At moderate swirl, the core of a pipe flow can be considered also as a model for turbulent transport in natural concentrated vortex. Thus, the results of investigation of turbulence structure in a pipe flow can be applied to a wide area of practical situations.

Despite the simple geometry of a pipe flow, there are great experimental difficulties associated with flow measurements even in the case of a non-rotating pipe. Therefore, correct flow modeling is important. Models developed for the velocity field in an isothermal turbulent flow can be further used for description of scalar fields. Such assumption, in the case of a pipe flow, is based on experimental data, which showed similarity of turbulent transport of velocity and scalar moments (Nagano and Tagawa (1988)), and that heat effects have no influence on the evolution of the velocity moment profiles under swirl (Sadovskii, 1991, Cannon et al., 1969).

As experiments demonstrate, it is possible to distinguish two regions in a rotating pipe flow with different structure of turbulence: the initial section of a pipe with a length of about $30D$ and the saturation region, which is observed at about $170D$ for a flow at any Reynolds number. In the former region, strong turbulence suppression is observed (Zaets et al., 1985). In the latter one, profiles of statistical characteristics reach their limit shapes (Kikuyama et al., 1983, Nishibori et al., 1987, and Imao et al., 1996, in particular).

The mean velocity components change monotonically along the pipe axis at the given swirl parameter and also at the given section with increasing a flow swirl. The profile of the longitudinal component tends to be parabolic as the one in a laminar flow, but does not reach such shape. The profile of the circumferential component has the parabolic limit shape $(W/W_o = (r/R)^2)$ instead of the expected linear one as it would be in the case of a forced rotational flow. Experiments also show that both limit profiles of U and W are not affected by the Reynolds number, and the profile of W does not depend on the value of the swirl parameter N. Turbulent friction decreases down to its limit value along the pipe. At the given section, turbulent friction decreases with increasing the swirl parameter.

However, we cannot use such notion as "laminarization of a flow under swirl", because moments of second and higher orders behave non-monotonically with increasing both parameters: pipe length and swirl degree. In the initial pipe section, strong suppression of moments is observed (Zaets et al., 1985). After suppression, moments of the second and higher orders increase and are stabilized at a high level (Zaets et al., 1985; Nishibori et al., 1987).

These and other features of a rotating pipe flow demonstrate how complex is its structure and that a good model of turbulence must reflect them.

The mathematical modeling of such flow with k–ε models does not give satisfactory results. In particular, for a developed rotating pipe flow, the k–ε model predicts a linear limit profile for W, as it would be in the case of solid body rotation, that is in contradiction with experimental data. The problem has its roots in the concept of turbulent viscosity (see. e.g., Torii and Yang, 1995).

In our research, two aims are pursued:

- to consider possibilities of some known Reynolds stress transport models to describe completely the turbulence structure of a pipe flow: initial region of strong turbulence suppression, the saturation region, and the transition area between them;
- to find how the turbulent diffusion model included in the RSTM influences the behavior of statistical characteristics in a swirling flow.

2. Verification of RSTMs in a pipe flow

2.1. Governing equations

The set of exact transport equations for the mean velocity vector and the turbulent stress tensor in the case of a stationary incompressible flow is written in the general tensor form as:

$$\begin{aligned} &U^j U_{i,j} = \nu g^{jk} U_{i,jk} - \langle u_i u^j \rangle_{,j} - \tilde{P}_{,i}/\rho \\ &U^i_{,i} = 0; \quad U^k \langle u_i u_j \rangle_{,k} = D_{ij} + P_{ij} + \Pi_{ij} - \varepsilon_{ij}, \end{aligned} \tag{1}$$

where $\varepsilon_{ij} = 2\nu g^{km} \langle u_{i,m} u_{j,k} \rangle$ is the dissipation tensor; $D_{ij} = -\langle u_i u_j u^m \rangle_{,m} - (\langle p u_i \rangle_{,j} + \langle p u_j \rangle_{,i})/\rho + \nu (g^{km} \langle u_i u_j \rangle_{,k})_{,m}$ is the diffusion term; $P_{ij} = -\langle u_j u^k \rangle U_{i,k} - \langle u_i u^k \rangle U_{j,k}$ is the production term; $\Pi_{ij} = \langle p(u_{i,j} + u_{j,i}) \rangle / \rho$ is the pressure–strain correlation.

To close set (1), terms D_{ij}, Π_{ij}, and ε_{ij} should be modeled.

2.2. Model approximations

On this stage of the research, the simple gradient diffusion model (Daly and Harlow, 1970) is used to model D_{ij} in each tested RSTM.

The dissipation tensor ε_{ij} is modeled by the isotropic expression with correction for low Reynolds numbers near a solid wall (So and Yoo, 1986). The equation for the dissipation rate of the kinetic turbulence energy is used in the following form (So and Yoo, 1986; Kurbatskii et al., 1995):

$$\begin{aligned} U^k \varepsilon_{,k} = &\left[g^{km} \left(\nu \varepsilon_{,k} + C_e \frac{k}{\varepsilon} \langle u_k u^l \rangle \varepsilon_{,l} \right) \right]_{,m} \\ &+ \left(C_{e1} P - C^*_{e2} \varepsilon \right) \frac{\varepsilon}{k} - \frac{2\nu\varepsilon}{x_n^2} f_1, \end{aligned} \tag{2}$$

$P = (1/2) P_{ii} = -\langle u_i u^k \rangle U_{i,k}$; f_1 and f_2 are damping functions (So and Yoo, 1986); C_e, C_{e1}, C_{e2}, C_{e3} are model constants, $C^*_{e2} = \max(1.4, C_{e2} f_2 (1 - C_{e3} \mathrm{Ri}))$ (Kurbatskii et al., 1995). The Richardson number characterizes influence of streamline curvature on turbulence like those of medium stratification on turbulent transport (Bradshaw, 1969). Eq. (2) at $\mathrm{Ri} = 0$ transforms into the "standard" equation.

Two model expressions for the pressure–strain correlation Π_{ij} were considered.

The first one (Launder et al., 1973) was taken with the wall correction (Gibson and Launder, 1978):

$$\Pi_{ij} = \Pi^{(1)}_{ij} + \Pi^{(2)}_{ij} + \left(\Pi'^{(1)}_{ij} + \Pi'^{(2)}_{ij} \right) f(x_n), \tag{3}$$

where

$$\Pi^{(1)}_{ij} = -C_1 \frac{\varepsilon}{k} \left(\langle u_i u_j \rangle - \frac{2}{3} \delta_{ij} k \right), \tag{4}$$

$$\Pi^{(2)}_{ij} = -C_2 \left(P_{ij} - \frac{2}{3} \delta_{ij} P \right), \tag{5}$$

$$\Pi'^{(1)}_{ij} = C'_1 \frac{\varepsilon}{k} \left(\langle u_n^2 \rangle g_{nn} \delta_{ij} - \frac{3}{2} \left(\langle u_n u_j \rangle g_{in} + \langle u_n u_i \rangle g_{jn} \right) \right), \tag{6}$$

$$\Pi'^{(2)}_{ij} = C'_2 \frac{\varepsilon}{k} \left(\Pi^{(2)}_{nn} g_{nn} \delta_{ij} - \frac{3}{2} \left(\Pi^{(2)}_{nj} g_{in} + \Pi^{(2)}_{ni} g_{jn} \right) \right) \tag{7}$$

$f = (1/5) k^{3/2} / (\varepsilon x_n)$ is a damping function, $C_1 = 1.5$, $C_2 = 0.6$, $C'_1 = C'_2 = 0.3$.

The other model expression for Π_{ij} was suggested in Launder (1989), where there was shown that in the case of an axisymmetric swirling flow, the convective transport tensor should be inserted in Eq. (5) to get better results:

$$C_{ij} = \frac{\partial}{\partial x_k}\left(U_k\langle u_i u_j\rangle\right) : \Pi_{ij}^{(2)} = -C_2\left(P_{ij} - C_{ij} - \frac{1}{3}\delta_{ij}(P_{kk} - C_{kk})\right). \quad (8)$$

Finally, verification of three RSTMs was carried out. Model 1 (denoted hereafter by M1), which was suggested in Kurbatskii et al. (1995), includes Eq. (2) ($\mathrm{Ri} \neq 0$) and model expressions (3)–(7) to close set (1). In the second model (M2), Eq. (2) at $\mathrm{Ri} = 0$ is used as well as expressions (3)–(7). At present, M2 is considered as the "standard" model and some of its properties have been analyzed for a turbulent flow in a rotating long cylindrical pipe in Hirai et al. (1989). Model 3 (M3) is similar to M2, but instead of expression (5), its modification (8) for a swirling flow is used.

2.3. Numerical procedure

In each model, the set of the closed equations for required functions (U, W, k, ε, $\alpha = \langle w^2\rangle - \langle v^2\rangle$, $\langle u^2\rangle$, and the other turbulent stresses) was written in the axisymmetric cylindrical frame of reference in the boundary layer approximation. The calculation conditions were the same as in the experiments (Zaets et al., 1985), where a swirling flow was obtained by conveying a fully developed turbulent flow ($U_o = 10^3$ cm/s, $\nu = 0.149$ cm^2/s, $u_{*o} = 43.5$ cm/s) from a stationary (non-rotating) straight cylindrical pipe of the 100-diameter length into a rotating cylindrical section of the same diameter ($D = 6$ cm). However, these conditions could be changed to get a flow with other parameters.

For solving the differential equations, the control volume technique (Spalding, 1977) was used. Boundary conditions were:

$$\frac{\partial U}{\partial r} = \frac{\partial k}{\partial r} = \frac{\partial \varepsilon}{\partial r} = \frac{\partial\langle u^2\rangle}{\partial r} = \frac{\partial \alpha}{\partial r} = \langle uv\rangle = \langle vw\rangle = \langle uw\rangle = W = 0 \quad (r = 0);$$

$$U = k = \varepsilon = \langle u^2\rangle = \alpha = \langle uv\rangle = \langle vw\rangle = \langle uw\rangle = 0, \quad W = W_o, \quad (r = R).$$

Profiles in the initial section of a stationary pipe flow were chosen as:

$$E(r) = E_o = 10^{-3}u_{*o}^2, \quad \langle u^2\rangle = (2/3)E_o, \quad \alpha = 0, \quad \langle uv\rangle = 0,$$

$$U(r) = \begin{cases} u_{*o}y_+, & 0 \leqslant y_+ \leqslant y_{+R}, \\ Au_{*o}(y_+)^{1/7}, & y_{+R} < y_+ \leqslant \mathrm{Re}_*, \ A = 8.74, \ y_{+R} = A^{7/6}. \end{cases}$$

The profile $\varepsilon(r) = \left(c_\mu f_\mu\right)^{1/2}E_o\partial U/\partial r$ was found from the local balance condition ($P = \varepsilon$) and from the gradient approximation $\langle uv\rangle = -c_\mu f_\mu(E^2/\varepsilon)\partial U/\partial r$, where $c_\mu = 0.09$ and $f_\mu = 1 - \exp(-0.01y_+)$ (So and Yoo, 1986). The pressure gradient in Eq. (1) was determined as

$$-\frac{1}{\rho}\frac{\mathrm{D}\tilde{P}}{\mathrm{D}x} = \frac{2}{R^2}\left(-r\left(\nu\frac{\partial U}{\partial r} - \langle uv\rangle\right)\Big|_0^R\right) = \frac{2\nu}{R}\left(-\frac{\partial U}{\partial r}\right)\Big|_{r=R}.$$

In the initial section, its value is known: $-(1/\rho)\left(\mathrm{D}\tilde{P}/\mathrm{D}x\right) = 2\left(u_{*o}^2/R\right)$.

The grid was non-uniform along r, with total number of nodes in this direction being 128. Size of δx was $0.05R$.

2.4. Results and discussion

Results of calculations were compared with experimental data. In experiments (Zaets et al., 1985), statistical characteristics (the first- and second-order moments of the velocity field) of a turbulent flow were measured in the exit section of short rotating pipe at $x/D = 25$, $\mathrm{Re_m} = 37000$, $N \leqslant 0.6$. In Kikuyama et al. (1983), Nishibori et al. (1987), and Imao et al. (1996), the behavior of the mean velocity components (longitudinal and circumferential) as well as the longitudinal turbulence intensity was studied in a long rotating cylindrical pipe ($x/D \leqslant 168$) at $\mathrm{Re_m} = 0.5 \sim 3 \cdot 10^4$ and $N = 0.5 \sim 3$. Because experiments were carried out under different conditions, quantitative comparison of the data is difficult.

As it was shown in Kurbatskii et al. (1995), M1 reproduces satisfactorily the evolutions of the U and W profiles, as well as the Reynolds stress profiles under moderate flow swirl ($N \leqslant 0.6$) in a short rotating pipe ($x/D = 25$). The present calculations carried out for a flow in a rotating long pipe, demonstrate that this model can catch only some features of the flow evolution downstream of the initial pipe section and only under moderate swirl ($N = 0.34$). It describes the decrease of the friction coefficient in consequence of laminarization of the longitudinal velocity profile (more exactly, its parabolization) and anisotropy of the kinetic turbulence energy components as well as tendency of the profiles of U and W to their limit shapes in the saturation region. However, these profiles are not in quantitative agreement with the experimental ones. Moreover, their dependence on both the Reynolds number and the swirl parameter is observed, and stabilization regime is reached at distances from the rotating pipe entrance much larger than it was obtained in experiments. At strong swirl ($N = 1$), the model does not describe turbulence structure adequately, that is, it predicts almost total suppression of turbulence in the section $x/D = 168$ in contradiction with the experimental data (Nishibori et al., 1987). The results of calculation of the damping coefficient of the longitudinal component of the turbulent kinetic energy calculated by M1, is shown in Fig. 1 as a function of the distance along the pipe axis.

Some results of calculations by M2 are also given in Fig. 1. The model does not describe correctly the behavior of the damping coefficient Ku and other statistical characteristics in a short pipe flow. However, a qualitative agreement is obtained for the increase of the turbulence intensities in the section $68 \leqslant x/D \leqslant 168$ of a long rotating pipe. The calculations indicate a dependence of the moments behavior on the Reynolds number at different pipe lengths and on swirl parameters in contradiction with experimental data. At high Reynolds numbers, the stabilization regime is not reached at all. So, the most known and simple variant of the RSTM does not describe correctly the flow structure.

The calculation results obtained by M3 are presented in Figs. 1–3. The profiles of the longitudinal and circumferential components of the mean flow velocity are shown at $x/D = 120$,

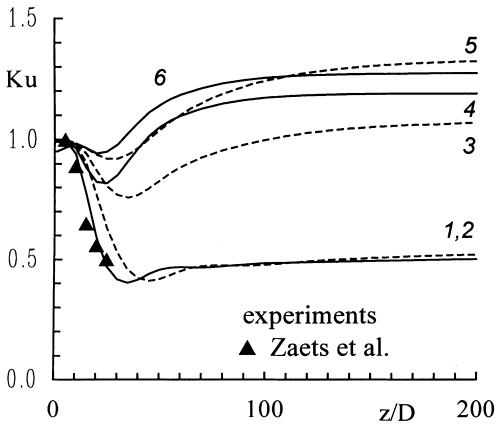

Fig. 1. Behavior of Ku along a pipe axis ($r/R = 0$, $N = 0.34$): (– – –) $\mathrm{Re_m} = 3.7 \cdot 10^4$; (——) $\mathrm{Re_m} = 10^4$ (curves 1,2: M1; 3,4: M2; 5,6: M3).

160 and compared with experimental data of Imao et al. (1996) and Kikuyama et al. (1983) at different swirl parameters. At moderate swirl, the model reproduces the evolution of the profile U along the pipe and gives its correct limit shape (Fig. 2). It is seen that in the stabilization regime, dependence of U on the Reynolds number is weak in accordance with experimental data. The profile of the circumferential velocity component (Fig. 3) reaches its limit parabolic shape at $N \leqslant 1$ and it does not depend on Re. Other statistical characteristics also reach their limit profiles, but their behavior along the pipe is not described correctly. In Fig. 1, the behavior of Ku obtained by M3, is shown as an example. For Ku, calculations demonstrate a weak dependence on the Reynolds number, and this dependence is observed in the whole pipe flow.

Thus, calculations demonstrate that RSTMs, even those modified specially for a swirling flow (Kurbatskii et al., 1995; Launder, 1989), can catch only some features of the flow structure and only under moderate swirl.

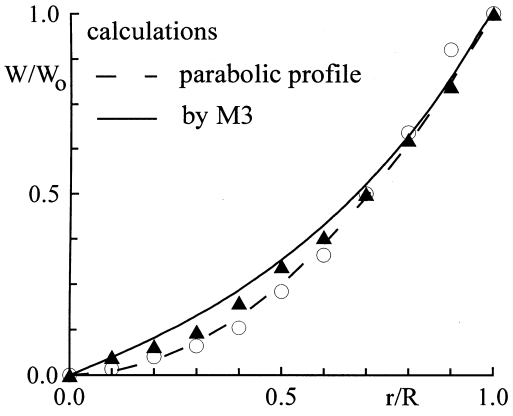

Fig. 3. Experimental data of Kikuyama et al. (1983) ($\mathrm{Re_m} = 10^4$, $3 \cdot 10^4$) and Imao et al. (1996) ($\mathrm{Re_m} = 2 \cdot 10^4$).

3. Turbulent diffusion models

Roots of shortcomings of RSTMs lie in models for pressure–strain correlations, dissipative tensor, and turbulent diffusion, if to stay in a frame of classical RSTMs. Contribution of models for each term should be estimated. In the present paper, the question how TDMs influence the results of calculations is studied, with models for dissipative tensor and pressure–strain correlations being considered as given. Taking into account that a pipe flow is inhomogeneous and that these are the third-order moments, which characterize the degree of flow inhomogeneity, it could be expected to improve results by using more correct model for turbulent diffusion. For example, some improvement has been got in such a way for a flow with buoyancy (Craft et al., 1997).

3.1. Verification of TDMs in a short pipe flow

At first, verification of some known models for turbulent diffusion (Daly and Harlow, 1970; Hanjalić and Launder, 1972; Dekeyser and Launder, 1983; Nagano and Tagawa, 1991) was carried out in a developed isothermal incompressible flow in a short rotating pipe ($x/D = 25$) at $\mathrm{Re_m} = 37000$. The model equations for the third-order velocity moments were solved in the output section of a pipe. The first- and second-order velocity moments necessary for calculation, were either obtained preliminarily by the Reynolds stress transport model (Kurbatskii et al., 1995) or taken from experiments (Zaets et al., 1985). In both cases, the results of calculations were compared with experimental data (Zaets et al., 1985; Karlsson et al., 1988; Fontaine and Deutsch, 1995). Comparison showed that no model can describe completely the behavior of the third-order moments over the whole pipe flow, from the axis to the wall, and under swirl (Poroseva, 1996; Kurbatskii and Poroseva, 1997). Therefore, a new model for the triple velocity correlations has been developed (Poroseva, 1996).

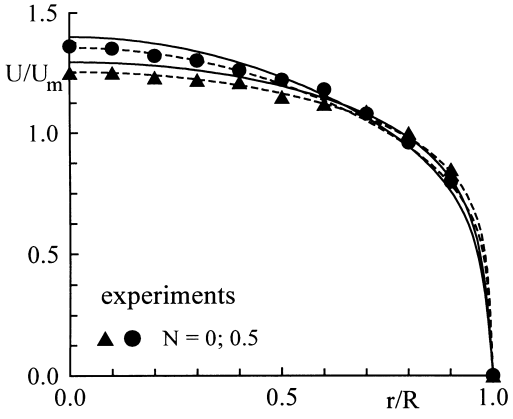

Fig. 2. Calculations by M3: (– – –) $\mathrm{Re_m} = 3.7 \cdot 10^4$, (——) $\mathrm{Re_m} = 10^4$. Experimental data of Kikuyama et al. (1983) ($\mathrm{Re_m} = 10^4$).

3.2. Present model

A new tensor-invariant model is derived from the exact transport equation for the triple velocity correlations:

$$\frac{\mathrm{D}\langle u_i u_j u_k\rangle}{\mathrm{D}t} = P_{ijk1} + P_{ijk2} + D_{ijk} + \Pi_{ijk} - \varepsilon_{ijk}, \tag{9}$$

where P_{ijk1} and P_{ijk2} are production terms due to Reynolds stresses interacting with their gradients as well as mean strains and do not need modelling, D_{ijk}, Π_{ijk}, and ε_{ijk} represent the terms of diffusion, pressure-containing correlation, and dissipation, respectively.

The production terms do not need modeling.

The advective term and ε_{ijk} are neglected. The dissipation term can be neglected in the assumption that the length scale of two-point velocity correlations is much less than that of the mean flow (Chou, 1945). Note that attempts to model ε_{ijk} were made, but we found that it does not influence the final result of modeling the triple velocity correlations.

For the pressure-containing correlation Π_{ijk}, the new tensor-invariant model expressions of "rapid" and "return-to-isotropy" parts are suggested.

Analyzing properties of the integral representation of $\langle u_i u_j p_{,k}\rangle$ obtained by solution of the corresponding Poisson equation for the pressure fluctuations, it is possible to derive the following expression for Π_{ijk}:

$$\Pi_{ijk} = -\frac{1}{\rho}\left(\langle u_i u_j p_{,k}\rangle + \langle u_j u_k p_{,i}\rangle + u_i u_k p_{,j}\rangle\right) = a^n_{mijk} U^m_{,n} + b_{ijk},$$

on the same assumption as it was done to exclude ε_{ijk} from Eq. (9). The general model form for the tensor function a^n_{mijk} in an incompressible flow reduces (Poroseva, 1996) to

$$a^n_{mijk} = C_3\left(\langle u_i u_j u_m\rangle\delta^n_k + \langle u_j u_k u_m\rangle\delta^n_i + \langle u_i u_k u_m\rangle\delta^n_j\right) + C_4\left(\langle u_i u_j u^n\rangle\delta_{km} + \langle u_j u_k u^n\rangle\delta_{im} + \langle u_i u_k u^n\rangle\delta_{jm}\right).$$

For the "return-to-isotropy" part of the correlation Π_{ijk}, the following model expression is suggested:

$$b_{ijk} = -\frac{\langle u_i u_j u_k\rangle}{C_{s3}\cdot\tau} + b_{ijkr}\langle u^t u^r\rangle_{,t}.$$

The general form for the tensor function b_{ijkr}, linear in the Reynolds stresses at a point and symmetric with respect to the rearrangement of index i, j, and k, can be written as

$$b_{ijkr} = C_6\big(\langle u_j u_k\rangle\delta_{ir} + \langle u_i u_j\rangle\delta_{kr} + \langle u_i u_k\rangle\delta_{jr}\big) + C_7\big(\langle u_j u_r\rangle\delta_{ik} + \langle u_i u_r\rangle\delta_{jk} + \langle u_k u_r\rangle\delta_{ij}\big) + C_8\big(\delta_{ik}\delta_{jr} + \delta_{ij}\delta_{kr} + \delta_{jk}\delta_{ir}\big)\cdot E.$$

Here, C_{s3} and $C_{3\text{–}8}$ are model constants obtained by comparing the calculated profiles with the experimental ones.

The model expression for the diffusion term D_{ijk} is derived using the quasinormality hypothesis that any fourth-order cumulants are zero and applying the high Reynolds number approximation:

$$D_{ijk} = -\big(\langle u_i u_j\rangle\langle u_k u^m\rangle + \langle u_j u_k\rangle\langle u_i u^m\rangle + \langle u_k u_i\rangle\langle u_j u^m\rangle\big)_{,m}.$$

The resulting model (named hereafter 'KP') includes ten model transport equations for the triple velocity correlations, which can be expressed one after another and solved in sequence.

Some results obtained by this model, e.g., for the skewness factor in the longitudinal direction in a rotating pipe flow, are presented in Fig. 4. In comparison with other TDMs, this model describes the turbulence structure in the whole pipe flow area and under swirl.

4. Calculations by the RSTM with different TDMs

4.1. Numerical procedure

For testing TDMs, we used the standard RSTM (M2) described in Section 2.2. Calculations were carried out at $\mathrm{Re}_o = (4\text{–}5)\cdot 10^4$.

For the turbulent diffusion term D_{ij}, several TDMs were sequentially introduced in Eq. (1). The best results have been got with ones suggested in Hanjalić and Launder (1972) and Poroseva (1996).

The former model (denoted as 'HL') is tensor-invariant and of the gradient type:

$$\langle u_i u_j u_k\rangle = -C_{s2}\cdot\tau\Big(\langle u^m u_j\rangle\langle u_i u_k\rangle_{,m} + \langle u^m u_i\rangle\langle u_j u_k\rangle_{,m} + \langle u^m u_k\rangle\langle u_i u_j\rangle_{,m}\Big) \quad (C_{s1} = 0.18).$$

Also, the result obtained by using the TDM (Daly and Harlow, 1970) will be discussed. This is the simplest model (denoted as 'DH')

$$\langle u_i u_j u_k\rangle = -C_{s1}\cdot\tau\Big(\langle u^m u_k\rangle\langle u_i u_j\rangle_{,m}\Big) \quad (C_{s1} = 0.22)$$

and therefore, is often used in practical calculations.

To make possible the application in the numerical procedure of any model for triple velocity correlations (see Section 2.3), we should leave D_{ij} in set (1) in its general form: $-\langle u_i u_j u^m\rangle_{,m}$. However, the price of generality of the procedure is a decrease of the forward-step size δx to $0.001R$ to avoid instability of the scheme, and it results in an essential increase of computer time. In this sense, further work is necessary to improve the procedure efficiency. Also, it was found that the differential equations for $\langle v^2\rangle$ and $\langle w^2\rangle$, rather than for k and α, should be solved to avoid non-physical oscillations of solution near the axis pipe, which appear in the latter case. The corresponding boundary conditions have been changed on $\partial\langle v^2\rangle/\partial r = \partial\langle w^2\rangle/\partial r = 0$ $(r = 0)$; $\langle v^2\rangle = \langle w^2\rangle = 0$ $(r = R)$.

4.2. Results and discussion

4.2.1. Stationary pipe flow

Calculations made with the DH-model, show that simple non-tensor-invariant model cannot describe correctly, in particular, the behavior of $\langle v^2\rangle$ and $\langle w^2\rangle$ near the pipe axis. The condition $\langle v^2\rangle = \langle w^2\rangle$ at $r = 0$ cannot be obtained, that is in contradiction with experimental data. Such problem did not appear in Hirai et al. (1989), and Kurbatskii et al. (1995), because the forced condition $\alpha = 0$ was used. Application of tensor-invariant models such as HL and KP has no such failing. Moreover, Figs. 5 and 6 show that the DH-model does not describe the behavior of the triple velocity correlations at all.

Models HL and KP are both tensor-invariant, but the former is of gradient type, whereas the latter not. Calculations demonstrate that to get the best results, the empirical coefficients C_1, C_2, and C_2' in model expressions for the pressure–strain correlation (4), (5), and (7) should be taken for both models equal to 1.7, 0.5, and 0.4, respectively, that is in agreement with conclusions of (Morris, 1984); coefficient C_d in the damping function f_1 (So and Yoo, 1986) should be chosen 1.0 instead of 0.5; $C_{e1} = 1.35$; $C_{e2} = 1.8$. The other constants

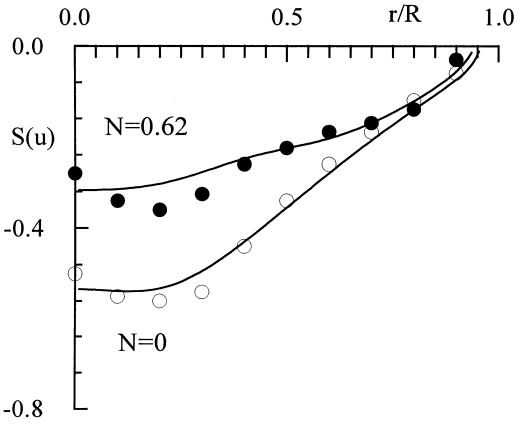

Fig. 4. Behavior of the longitudinal skewness factor under swirl obtained by the KP-model. Experimental data of Zaets et al. (1985).

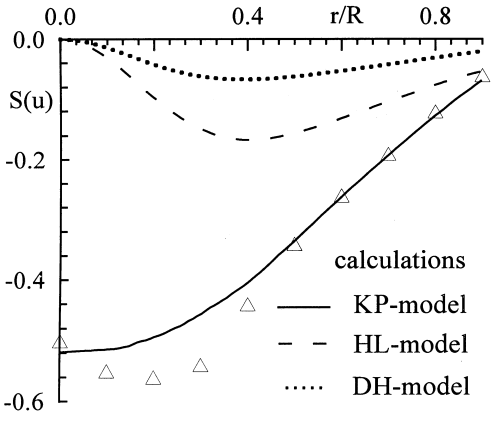

Fig. 5. Profiles of the longitudinal skewness factor in a stationary pipe flow.

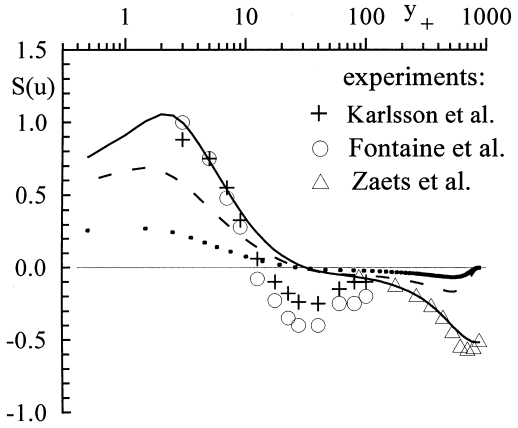

Fig. 6. Profiles of the longitudinal skewness factor in a stationary pipe flow.

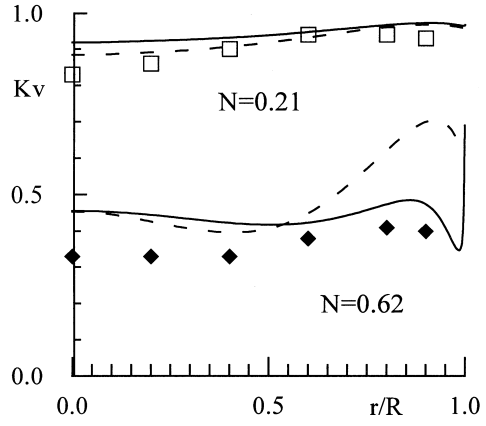

Fig. 8. Calculated profiles: (– – –) Kurbatskii et al. (1995), (——) with using the HL-model. Experimental data of Zaets et al. (1985).

were the following. For the HL-model: $C_1' = 0.4$, $C_e = 0.25$, $C_{s2} = 0.18$ (instead of 0.11 usually used). For the KP-model: $C_1' = 0.3$, $C_e = 0.3$, $C_{s3} = 0.12$, $C_3 = 0.1$, $C_4 = 0.8$, $C_6 = -1.2$, $C_7 = -0.2$, $C_8 = 0.4$.

Some results are presented in Figs. 5 and 6. Note that experimental data shown in figures were obtained at different values of the momentum thickness Reynolds number, so, the comparison can be only qualitative. The KP-model gives good results for the triple velocity correlations in the whole flow area, whereas the HL-model does not describe a wall area and gives the zero value of $S(u)$ on the pipe axis in contradiction with the experimental data. For the other triple velocity correlations in the flow core, this model gives results quantitatively comparable with the ones obtained by the KP-model.

However, for reproducing the behavior of the second-order moments as well as the mean velocity components, the important characteristic of the applied TDM is its tensor-invariance. Moreover, in any case the damping functions as wall corrections should be kept both in the ε-equation and in the model expression for the pressure–strain correlation.

4.2.2. Rotating pipe flow

Under swirl, tensor-invariant TDMs give better results. Some profiles obtained by the RSTM with HL-model are shown in Figs. 7 and 8 at $x/D = 25$. They are compared with the data (Kurbatskii et al., 1995), where the DH-model was applied to model turbulent diffusion. The difference is strong especially near the wall and increases with swirl increasing.

To describe the initial section of a rotating pipe flow, we kept modification of Eq. (2) by Richardson number ($\mathrm{Ri} = 2.$), but the results for Ku in Fig. 9 were obtained at $\mathrm{Ri} = 0$. More experimental data are necessary to understand if we should apply such modification or not, because in experiments (Zaets et al., 1985; Nishibori et al., 1987), the different degree of turbulence suppression was obtained in the initial pipe section.

Profiles calculated with the use of KP- and HL-models are close and with increasing both swirl and Reynolds number, the difference between them becomes less. Also, the HL-model gives more stable results at different values of the swirl number. So, we come to a paradoxical conclusion that a less correct TDM is preferable at present for practical calculations. The reason lies in incorrect modeling the other terms in set (1).

In a long rotating pipe, the standard RSTM with the tensor-invariant TDM describes the behavior of the second-order moments in the saturation regime (Fig. 9). In spite of this, profiles of the mean velocity components are reproduced worse (Fig. 10) than by M3 (Fig. 2). It shows that mean velocity profiles are influenced, in the main, by the model expression for the pressure–strain correlations.

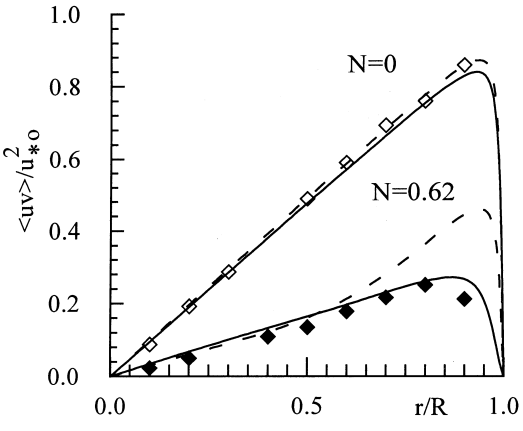

Fig. 7. Calculated profiles: (– – –) Kurbatskii et al. (1995); (——) with using the HL-model. Experimental data of Zaets et al. (1985).

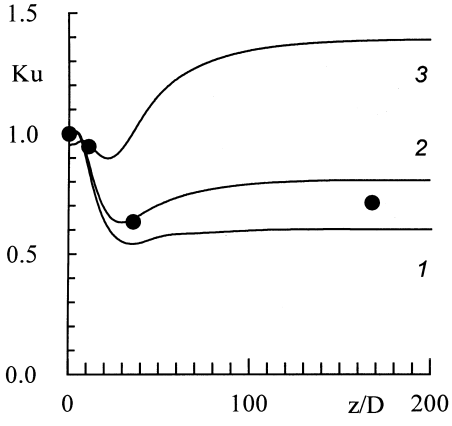

Fig. 9. Calculated profiles obtained with the use of KP-model (curve 1), HL-model (curve 2), and by M3 (curve 3). Experimental data of Nishibori et al. (1987) ($N = 0.5$, $\mathrm{Re_m} = 3 \cdot 10^4$).

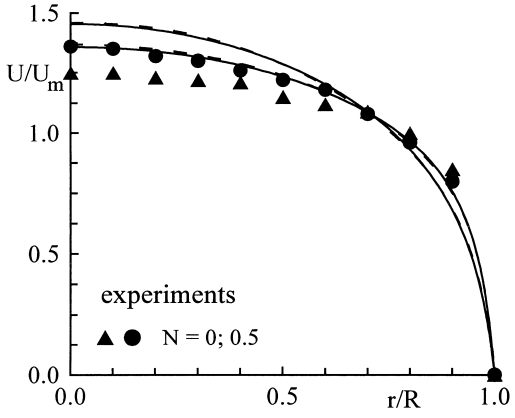

Fig. 10. Profiles of the longitudinal mean velocity component. Experimental data of Kikuyama et al. (1983) ($Re_m = 10^4$). Calculated profiles obtained with using KP (– – –) and HL (——) models.

5. Conclusion

The structure of a turbulent flow in a rotating cylindrical pipe undergoes a complicated evolution along the pipe axis. The calculations demonstrate that RSTMs, even those modified specially for a swirling flow, cannot describe a flow structure completely.

To calculate the first- and second-order velocity moments in a swirling flow of practical interest, the main condition for a TDM used is its tensor-invariance, and the model (Hanjalić and Launder, 1972) is the best choice at present. This model is simple and gives stable results at different swirl numbers. Application of more correct TDM though results in improved description of the first- and second-order moments evolution in a flow under swirl, but this improvement is not cardinal and the difference in the results obtained by two TDMs decreases with increasing the swirl parameter. Even if tensor-invariant TDMs are used, we should keep in the RSTM the damping functions as wall correction, and the Richardson number to describe turbulence suppression in a short rotating pipe.

The evolution of the mean velocity components are influenced by the model expression for the pressure–strain correlations, rather than the TDM. However, the use of more accurate TDMs, such as suggested, for instance, in Poroseva (1996), gives a possibility to develop more physically correct models for these correlations as well as for dissipation tensor and, finally, get the RSTM, which will be possible to apply a wider range of flows. Such model can be also used for researching turbulent transport of components of the turbulent kinetic energy as well as developing models for heat and mass transport.

Acknowledgements

This work was supported by the Russian Foundation of Basic Research under grant N 96-02-16001.

References

Bradshaw, P., 1969. The analogy between streamline curvature and buoyancy in turbulent shear flow. J. Fluid Mech. 36, 177–191.

Cannon, J.N., Kays, W.M., 1969. Heat transfer to a fluid flowing inside a pipe rotating about its longitudinal axis. ASME J. Heat Transfer 92, 135–140.

Chou, P.Y., 1945. On velocity correlations and the solutions of the equations of turbulent fluctuation. Q. Appl. Math. 3 (1), 38–54.

Craft, T.J., Kidger, J.W., Launder, B.E., 1997. Importance of third-moment modeling in horizontal, stably-stratified flows. In: Proceedings of Turbulent Shear Flows 11, 13–18.

Daly, B.J., Harlow, F.H., 1970. Transport equations in turbulence. Phys. Fluids 13 (11), 2634–2649.

Dekeyser, I., Launder, B.E., 1983. A comparison of triple-moment temperature–velocity correlations in the asymmetric heated jet with alternative closure models. In: Turbulent Shear Flows 4. Springer, Berlin, pp. 102–117.

Fontaine, A.A., Deutsch, S., 1995. Three-component, time-resolved velocity statistics in the wall region of a turbulent pipe flow. Experiments in Fluids 18, 168–173.

Gibson, M.M., Launder, B.E., 1978. Ground effects on pressure fluctuations in the atmospheric boundary layer. J. Fluid Mech. 86, 491–511.

Hanjalić, K., Launder, B.E., 1972. A Reynolds stress model of turbulence and its application to thin shear flows. J. Fluid Mech. 52, 609–638.

Hirai, S., Takagi, T., Matsumoto, M., 1989. Contribution towards a Reynolds-stress closure for low-Reynolds-number turbulence. Trans. JSME 52 (476), 1608–1616.

Imao, S., Itoh, M., Harada, T., 1996. Turbulent characteristics of the flow in an axially rotating pipe. Int. J. Heat Fluid Flow 17 (5), 444–451.

Karlsson, R.I., Johansson, T.G. 1988. LVD measurements of higher order moments of velocity fluctuations in a turbulent boundary layer. In: Laser Anemometry in Fluid Mechanics. Ladoan Instituto Superior Tecnico, Lisbon.

Kikuyama, K., *et al.*1983. Flow in an axially rotating pipe (a calculation of flow in the saturated region). Bull. JSME 26 (214), 506–513.

Kurbatskii, A.F., Poroseva, S.V., Yakovenko, S.N., 1995. Calculation of statistical characteristics of a turbulent flow in a rotated cylindrical pipe. High Temperature 133 (5), 738–748.

Kurbatskii, A.F., Poroseva, S.V., 1997. Turbulence model for the triple velocity correlations. In: Proceedings of The Seventh Int. Symp. on Computational Fluid Dynamics, Beijing, China, pp. 435–439.

Launder, B.E., Reece, G.J., Rodi, W., 1973. Progress in the development of a Reynolds stress turbulent model. J. Fluid Mech. 68, 537–566.

Launder, B.E., 1989. Second-moment closure and its use in modeling turbulent industrial flows. Int. J. Numer. Methods Fluids 9, 963–985.

Morris, P.J., 1984. Modeling the pressure redistribution terms. Phys. Fluids 27 (7), 1620–1623.

Nagano, Y., Tagawa, M., 1988. Statistical characteristics of wall turbulence with a passive scalar. J. Fluid Mech. 196, 157–185.

Nagano, Y., Tagawa, M., 1991. Turbulence model for triple velocity and scalar correlations. In: Turbulent Shear Flows 7. Springer, Berlin, pp. 47–62.

Nishibori, K., Kikuyama, K., Murakami, M., 1987. Laminarization of turbulent flow in the inlet region of an axially rotating pipe. Bull. JSME 30 (260), 255–262.

Poroseva, S.V., 1996. Model of higher-order velocity moments transport for a developed turbulent flow in a cylindrical pipe (in Russian). Ph.D. Thesis, Novosibirsk State University.

Sadovskii, M.V., 1991. Research on the behavior of probability density distribution and velocity and temperature fluctuation spectra in a turbulent flow in a rotating pipe by thermoanemometric technique (in Russian). Ph.D. Thesis, Moscow Physics and Technics Institute.

So, R.M.C., Yoo, G.J., 1986. On the modeling of low-Reynolds-number turbulence. NASA Contractor Report 3994.

Spalding, D.B., 1977. GENMIX: a General Computer Program for Two-Dimensional Parabolic Phenomena. Pergamon Press, New York.

Torii, S., Yang, W., 1995. Numerical prediction of fully developed turbulent swirling flows in an axially rotating pipe by means of a modified k–ε turbulence model. Int. J. Numer. Methods Heat Fluid Flow 5, 175–183.

Zaets, P.G., Safarov, N.A., Safarov, R.A., 1985. Experimental study of the turbulence characteristics behavior under rotating a pipe around its longitudinal axis (in Russian). In: Modern Problems of Continuous Medium Mechanics. Moscow Physics and Technics Institute, pp. 136–142.